Video Article

Protocol for the Evaluation of MRI Artifacts Caused by Metal Implants to Assess the Suitability of Implants and the Vulnerability of Pulse Sequences

Tim Hilgenfeld[1], Marcel Prager[1], Franz S. Schwindling[2], Johann M.E. Jende[1], Peter Rammelsberg[2], Martin Bendszus[1], Sabine Heiland[1], Alexander Juerchott[1]

[1]Department of Neuroradiology, Heidelberg University Hospital

[2]Department of Prosthodontics, Heidelberg University Hospital

Correspondence to: Alexander Juerchott at alexander.juerchott@med.uni-heidelberg.de

URL: https://www.jove.com/video/57394
DOI: doi:10.3791/57394

Keywords: Engineering, Issue 135, Susceptibility artifacts, implants, pulse sequence, magnetic resonance imaging, metal, artifact size, magnetic susceptibility

Date Published: 5/17/2018

Citation: Hilgenfeld, T., Prager, M., Schwindling, F.S., Jende, J.M., Rammelsberg, P., Bendszus, M., Heiland, S., Juerchott, A. Protocol for the Evaluation of MRI Artifacts Caused by Metal Implants to Assess the Suitability of Implants and the Vulnerability of Pulse Sequences. *J. Vis. Exp.* (135), e57394, doi:10.3791/57394 (2018).

Abstract

As the number of magnetic resonance imaging (MRI) scanners and patients with medical implants is constantly growing, radiologists increasingly encounter metallic implant-related artifacts in MRI, resulting in reduced image quality. Therefore, the MRI suitability of implants in terms of artifact volume, as well as the development of pulse sequences to reduce image artifacts, are becoming more and more important. Here, we present a comprehensive protocol which allows for a standardized evaluation of the artifact volume of implants on MRI. Furthermore, this protocol can be used to analyze the vulnerability of different pulse sequences to artifacts. The proposed protocol can be applied to T1- and T2-weighted images with or without fat-suppression and all passive implants. Furthermore, the procedure enables the separate and three-dimensional identification of signal loss and pile-up artifacts. As previous investigations differed greatly in evaluation methods, the comparability of their results was limited. Thus, standardized measurements of MRI artifact volumes are necessary to provide better comparability. This may improve the development of the MRI suitability of implants and better pulse sequences to finally improve patient care.

Video Link

The video component of this article can be found at https://www.jove.com/video/57394/

Introduction

MRI has become an indispensable diagnostic tool. As a result, the number of MRI systems used in routine diagnostics is further increasing[1]. At the same time, the number of patients with implants is increasing as well[2,3]. In 2012, for instance, more than 1 million knee and joint replacements have been performed in the USA alone[4]. The prevalence of such implants was about 7 million in 2010, which corresponds to more than 10% of females in the age group 80-89 years[5]. As a result, the image quality and the diagnostic significance of MRI examinations are often impaired by artifacts due to metallic implants, resulting in a decreased diagnostic accuracy. Therefore, the MRI suitability of implants and the artifact vulnerability of pulse sequences are becoming increasingly important. Numerous approaches have been published to evaluate these characteristics. Due to strong discrepancies in the used evaluation methods, however, the respective results are hard to compare.

An evaluation of the MRI suitability of materials can be performed by calculating their magnetic susceptibility[6]. However, the vulnerability of different pulse sequences to artifacts cannot be compared with that approach for a given implant. *Vice versa*, the artifact volumes for a given pulse sequence can only be roughly estimated for different implants. In addition, the analysis is often performed with artificially shaped implants[7,8]. As the material volume and shape have an influence on the artifact size[6], these features should be taken into account as well. As an alternative to magnetic susceptibility, the artifact size can be evaluated. Frequently, studies only rely on the qualitative evaluation of the artifact size[9] or focus on the two-dimensional artifact size only covering one slice of the implant artifact[10,11]. Moreover, manual segmentation approaches are often used, which is not only time-consuming but also prone to intra- and inter-reader differences[11]. Finally, protocols often do not allow to test for non-fat-saturated and fat-saturated sequences at the same time[12]. This, however, would be desirable, since the applied fat suppression technique profoundly affects the artifact size.

Here, we present a protocol which allows for the reliable, semiautomatic, threshold-based, three-dimensional quantification of signal loss and pile-up artifacts of the entire implant, or all slices containing visible implant artifacts. Furthermore, it allows for testing T1- and T2-weighted images with or without fat-saturation. The protocol can be used to evaluate the MRI suitability of different implants or the vulnerability of different pulse sequences to metallic artifacts for a given implant.

Protocol

1. Phantom Preparation

1. Determine the implant volume (*e.g.*, by using the water displacement method).
   NOTE: The volume of the CCT-T sample and the Z-T sample measured 0.65 mL and 0.73 mL, respectively.
2. Fix the implant position in the middle of a non-ferromagnetic, plastic, waterproof box by using a thin thread. Use a box that is larger than the expected MRI artifacts.
   NOTE: If no rough estimates of the artifact volumes of the implant and/or pulse sequence of interest are available, perform a test scan by placing the phantom in a box, approximately 10x larger than the phantom, filled with water. The artifact volumes in this study ranged from 7.3 mL (for the CCT-T sample) and 0.09 mL (for the Z-T sample).
3. **Carefully melt a mixture of semisynthetic fat (58.8%), water (40%), and macrogol-8-stearate (1.2%), using a water bath at 50 °C.**
   NOTE: For the samples in this study, we used a 500 mL mixture for the embedding of each sample.
   1. When the mixture becomes fluid, stop heating and start with slow stirring, and stop heating. Ensure that there is no separation of the fat and water phases.
4. As soon as clotting begins, slowly start embedding the implant with the mixture. For this, pour the embedding mixture slowly into the phantom box with the implant.
   NOTE: Pouring must be performed slowly to avoid air inclusion.
5. Place the phantom box with the embedded implant into the refrigerator at 4 °C overnight for desiccation. The next day, remove any residual fluid parts by decantation.

2. MRI Examination

1. Place the phantom (box with the embedded implant) in the MRI in the same orientation as in the *in vivo* situation. Position the middle of the phantom in the isocenter of the MRI.
2. For measurements, use a coil which allows for a homogeneous signal distribution within the imaging volume without severe and obvious signal drops (*e.g.*, a head coil).
3. When planning the MRI scans at the MRI console, ensure that the phantom box, including some air at the edges of the box, is within the imaging volume.
4. Next, perform the MRI examination.

3. Image Analysis and Post-processing

1. Export the images without any loss of quality (*e.g.*, by compression) from the MRI console (*e.g.*, using the DICOM format). Import the images in an MRI post-processing software which allows for placing the region of interests (ROI), evaluating ROI signal intensities, a threshold-based segmentation, and a quantification of the segmentation volumes (see **Table of Materials**).
2. **To define the threshold for pile-up artifacts and check for a homogeneous signal distribution within the imaging volume, place lines perpendicular to each other and adjacent to the outer border of the visible artifact on the slice with the maximum artifact size (Figure 1a).**
   NOTE: Pile-up artifacts are displacement artifacts, presenting with areas with artificially high signal intensities. They occur in the slice direction and the readout direction.
   1. Place a background ROI ($ROI_{Background}$) with 10 mm in diameter outside each of the four intersection points (**Figure 1a**). Place the lines and the background regions of interests using the segmentation editor.
   2. Measure the mean signal intensity and standard deviation (SD) of all voxels within these 4 $ROI_{Background}$ values and for each $ROI_{Background}$ separately. Use the tool **Material Statistics** in the project view.
   3. Ensure that the mean signal intensity of each $ROI_{Background}$ is within the range of ± 1.5 SD of the mean signal of each of the other 3 counterparts to guarantee a homogeneous signal distribution.
   4. Calculate the threshold for pile-up artifacts by adding 3 SD of $ROI_{Background}$ to the mean signal intensity of all voxels of these 4 $ROI_{Background}$ values. Perform a semiautomatic threshold-based segmentation of pile-up artifacts by selecting all voxels with the signal intensities larger than the threshold adjacent to the signal loss artifact in every slice. Use the masking tool of the segmentation editor to visualize the predefined signal intensity range and restrict the segmentation to it.
3. **To define the threshold for signal loss artifacts, place 4 regions of interests (ROIs) in air-containing regions (ROI_{Air}; each 10 mm in diameter) at the corners of the phantom box and measure the mean signal intensity and SD of all voxels within these 4 ROI_{Air} as described in step 3.2, using the segmentation editor and "Material Statistics", respectively.**
   NOTE: Signal loss artifacts present with voxels having artificial low signal intensities. They are caused by dephasing and displacement artifacts.
   1. Place an ROI in the core of the signal loss artifact (ROI_{Core}) defined by the largest connected area of low signal intensities (**Figure 1a**). Manually increase the size of the ROI_{Core} until the largest possible size within the signal loss artifact whose mean signal intensity is lower than the mean ROI_{Air} + 3x of the respective SD is found. Finally, measure the mean signal intensity and SD of the ROI_{Core}.
   2. Calculate the signal intensity threshold for signal loss artifacts by adding 3 SD of the ROI_{Core} to the mean of the ROI_{Core}. Perform a semiautomatic threshold-based segmentation of signal loss artifacts by selecting all voxels connected to the ROI_{Core} with signal intensities below the threshold.

3. Use the masking tool of the segmentation editor to visualize the predefined signal intensity range and restrict the segmentation to it. If possible, use the "Fill" function in the tap "Selection" of the segmentation editor to include all voxels within the segmentation that are not yet selected. If applicable, manually add the additional unequivocal signal loss artifacts to the segmentation.

4. Subtract the physical implant volume from the calculated artifact volume to obtain the true artifact volume. Repeat the analysis at least 3x. A time interval of at least two weeks should separate the multiple reads to exclude a learning bias.

Representative Results

With the above-mentioned protocol, we evaluated the artifact volume of 2 different dental implants made of Titanium (T; see the **Table of Materials**) supporting different crowns [porcelain-fused-to-metal non-precious alloy (CCT-T) and monolithic zirconia (Z-T); **Figure 1b** and **1c**]. The CCT-T sample represents a highly paramagnetic material composition predicting large artifacts (Cobalt 61%, Chrome 21%, and Tungsten 11%; CCT). The crown material of the Z-T sample represents a low paramagnetic material (Zirconia 92%; Z). Furthermore, four different, non-fat-saturated, T2-weighted sequences were evaluated to compare their vulnerability to metal artifacts. Specifically, the techniques of multiple slab acquisition with a view-angle-tilting gradient based on a sampling perfection with application-optimized contrasts using different flip angle evolutions (MSVAT-SPACE), slice encoding for metal artifact correction (SEMAC), and their conventional counterparts SPACE and turbo spin echo (TSE) were evaluated (see **Table 1** for the detailed sequence parameters). MRI scans were performed on a 3T MRI system (see the **Table of Materials**) and a 16-channel multipurpose surface coil was used. The variation of the pulse sequence parameters has a strong impact on the artifact size. Thus, pulse sequence parameters were chosen as close as possible to those used in the *in vivo* dental MRI scans to increase the transferability of the results. The analysis was performed 3x by two independent raters. For multiple comparisons, a two-way analysis of variances and *post hoc* Tukey tests were used.

The data analysis reveals differences between both samples and the applied sequences. In all sequences, the combined artifact volumes (the sum of the signal loss and pile-up) of the CCT-T sample were larger compared to the Z-T sample (P <0.001; **Figure 2** and **Figure 3**). Within the same sequence, the artifact volume of the CCT-T sample was 19.3x (SEMAC) to 39.6x (MSVAT-SPACE) larger than the artifact volume of the Z-T counterpart.

The choice of pulse sequence had a significant impact on the artifact volume as well (**Figure 2** and **Figure 3**). Regarding the CCT-T sample, the smallest artifact volumes were observed for TSE and SEMAC, and the largest artifacts for SPACE (P <0.001). In addition, MSVAT-SPACE significantly reduced the artifact volume compared to SPACE (P <0.001; 3.8 *vs.* 7.3 mL). In contrast, no significant differences were observed between MSVAT-SPACE, TSE, and SEMAC for the Z-T sample. The artifact volume for Z-T was largest in SPACE and was significantly reduced by MSVAT-SPACE (P <0.05; 0.26 *vs.* 0.1 mL).

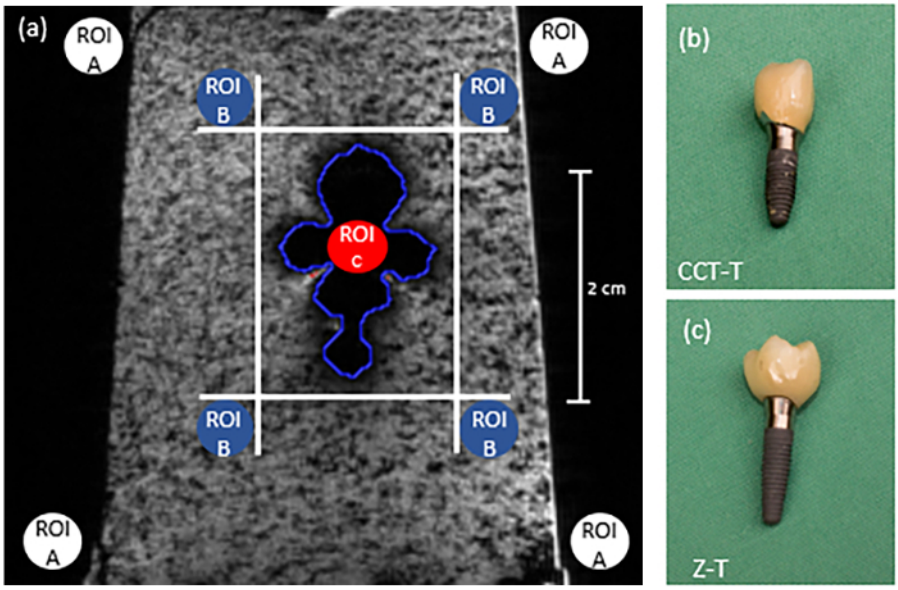

Figure 1: ROI positioning and implant samples. (**a**) This panel shows a typical positioning of the regions of interests (ROIs) for measuring the thresholds for pile-up artifacts and signal distribution (ROI_B = $ROI_{Background}$) and signal loss artifacts (ROI_A = ROI_{Air}; ROI_C = ROI_{Core}). The blue contour resembles the result of the semiautomatic segmentation for signal loss artifacts within that slice. The small red areas correspond to the result of pile-up artifacts. (**b** and **c**) These panels show images of used dental implants supporting different single crowns. Cobalt-Chromium-Tungsten-Titanium (CCT-T); Zirconia-Titanium (Z-T). Please click here to view a larger version of this figure.

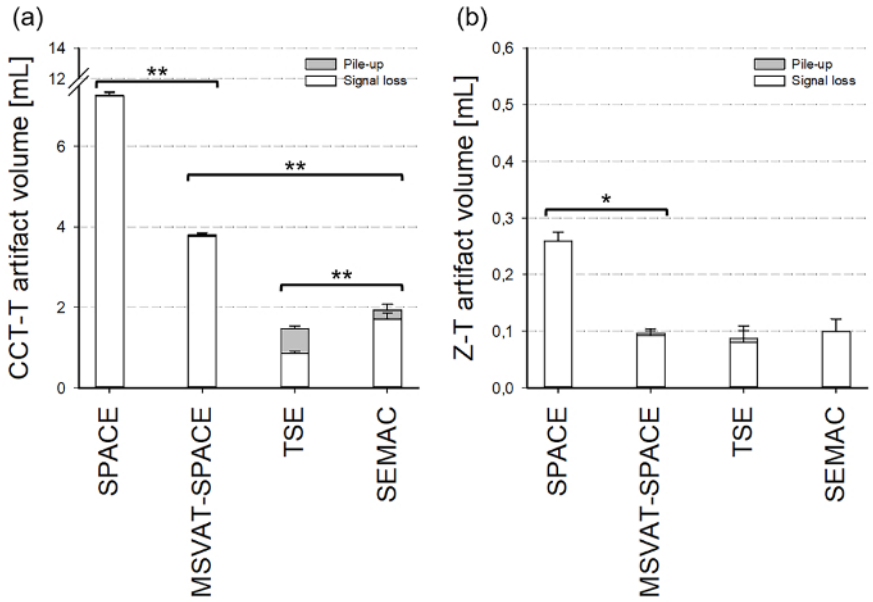

Figure 2: Artifact volume measurements. (**a** and **b**) These are bar graphs showing the mean values with the standard deviations of the three-dimensional artifact volume of the entire implant samples for all 4 evaluated sequences after subtracting the physical implant volume. If applicable, separate standard deviation error bars are given for signal loss and pile-up artifacts. * $P \leq 0.05$; ** $P \leq 0.001$ Please click here to view a larger version of this figure.

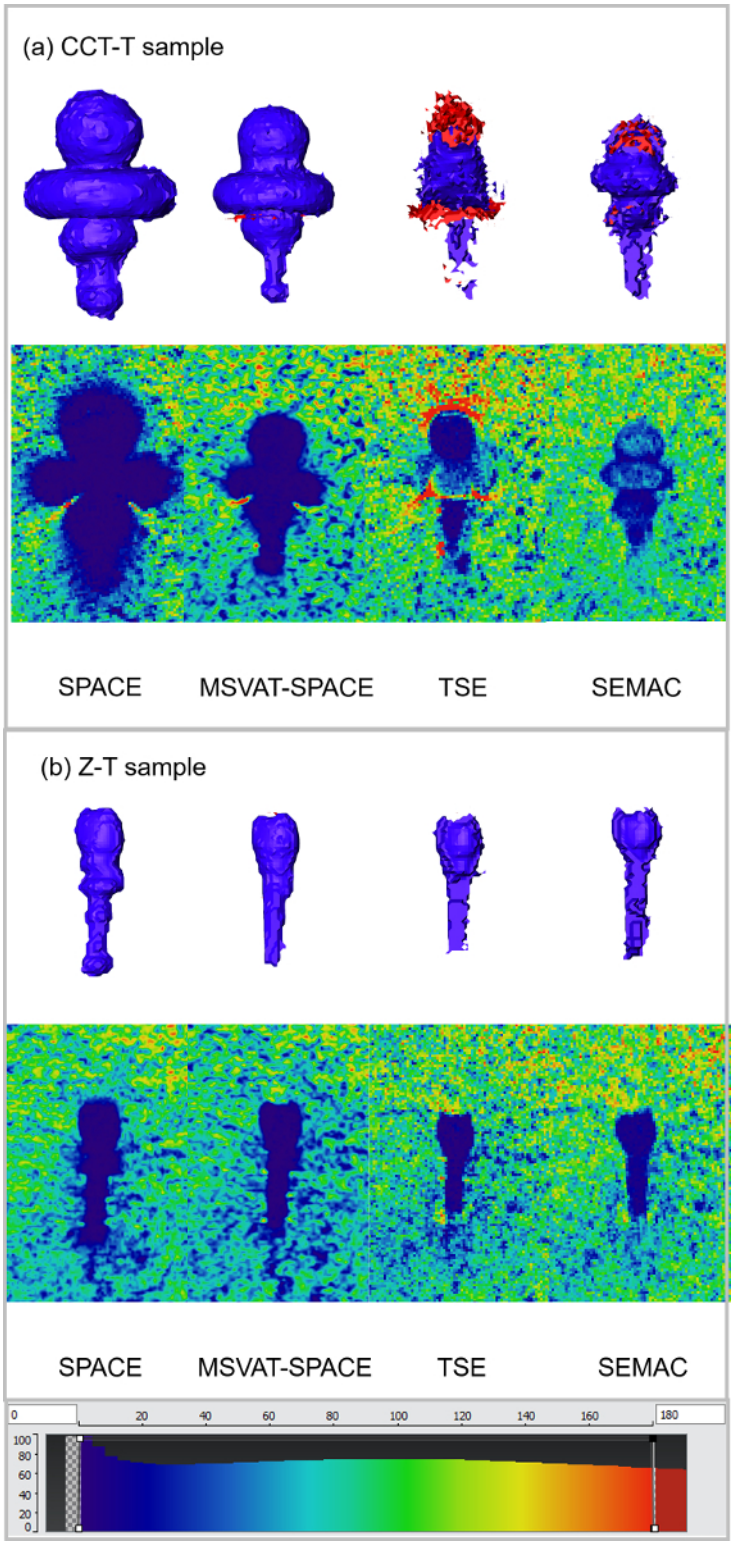

Figure 3: Appearance of artifacts. These panels render the artifact volumes of the entire implants (upper row). The blue colored areas represent signal loss artifacts and the red colored areas represent pile-up artifacts. The panels show the colored source images (lower row) for all evaluated T2-weighted sequences. Panel (**a**) is of the Cobalt-Chromium-Tungsten-Titanium (CCT-T) sample and panel (**b**) is of the Zirconia-Titanium (Z-T) sample. Please click here to view a larger version of this figure.

Sequence	TR/TE [ms]	Voxel size [mm^3]	FOV [mm^2]	Matrix	Readout Bandwidth [Hz/Px]	Slices	Slice encoding steps or oversampling [%]	VAT	Time [min:sec]
SPACE	2,500/131	0.55 x 0.55 x 0.55	140 x 124	256 x 256	501	72	55.6	No	14:02
MSVAT-SPACE	2,500/199	0.55 x 0.55 x 0.55	140 x 84	256 x 256	528	72	55.6	Yes	6:04
TSE	5,100/44	0.59 x 0.59 x 1.5	150 x 150	256 x 256	592	25	No	No	3:36
SEMAC	5,100/45	0.59 x 0.59 x 1.5	150 x 150	256 x 256	592	25	4	Yes	6:19

Table 1: Parameters of all used sequences.

Discussion

The number of patients with metallic implants and the number of MRI examinations is currently increasing[1,2,3]. In the past, MRI examinations were avoided after joint replacements. Today, however, MRI is not only requested for imaging such patients but should also allow for the evaluation of complications directly adjacent to joint arthroplasty. Thus, the MRI safety and MRI suitability of implants, as well as the robust pulse sequences for metal artifact suppression, are becoming increasingly important[13]. For the evaluation of MRI suitability in terms of artifact volume, we present a comprehensive, time-efficient protocol. It allows for a reliable, three-dimensional evaluation of signal loss and pile-up artifacts as an indicator of slice distortions for fat-suppressed and non-fat-suppressed T1- and T2-weighted pulse sequences.

For some protocol steps, special attention is necessary to achieve the best possible result. After melting the embedding substance and before embedding the implant, it is very important to stir the embedding substance long enough while it starts cooling down and its aggregate state changes (fluid to solid), as its fat and water phases easily separate, even in the presence of an emulsifying agent. Furthermore, it is important to slowly fill the phantom box with the embedding substance to avoid air bubbles. This is crucial because air and signal loss artifacts both result in zero signal, which would lead to an overestimation of the artifact.

A high and homogeneous signal is necessary to allow for an accurate evaluation of the artifact volume. If the highest signal-to-noise ratio (SNR) is achieved by surface coils, it is crucial to test beforehand that the sensitivity of the profile and the coil positioning allows for a homogeneous signal within the phantom (as described above), so that the threshold-based segmentation can run without any segmentation errors.

Compared with other studies analyzing large implants (*e.g.*, hip or knee replacements or spondylodesis), this protocol used small implants, in some cases causing artifact volumes far below 1 mL. Even under such challenging conditions, we could detect significant differences in the artifact volumes between different samples and different pulse sequences. Thus, a high measurement accuracy of this protocol can be assumed, allowing for an accurate evaluation of the MRI artifact volume of complex implants with regard to their material composition and shape. Moreover, the protocol can be applied to compare the vulnerability of different pulse sequences to metal-induced artifacts caused by a given implant.

Numerous methods with different complexity have been suggested for the evaluation of metallic artifacts. For the comparison of different pulse sequences, Fritz *et al.* used a qualitative ranking to evaluate the vulnerability of each sequence[11]. Others, such as Zho *et al.*, determined in plane artifact (signal loss and pile-up) volumes by measuring the greatest distance and through plane artifacts by counting the number of slices being affected by artifacts[10]. Both methods, however, do not consider the full artifact volume, which may result in the under- or overestimation of artifact volume. That also applies to some studies that used manual segmentation[11]. Because this is a very time-consuming approach, often only one or two central slices are evaluated on a visual basis, neglecting the remaining artifact proportions.

For *in vitro* studies, authors often use agarose or gelatin as the embedding substance[14,15]. Both materials can be handled easily and guarantee enough signal in T2- and T1-weighted images. However, they do not allow for the evaluation of fat-suppressed sequences in any weighting. This represents a major drawback, since fat suppression has a profound impact on the artifact volume and is used regularly to identify implant-related complications (*e.g.*, edema and fluid collections adjacent to the implant in cases of infection, particle disease, or aseptic lymphocyte-dominated vasculitis-associates lesion)[13,16,17].

Some limitations of this protocol must be acknowledged. First, it does not allow *in vivo* quantification of the artifact volume, as the differentiation of the complete artifact volume requires a homogeneous background signal. For *in vivo* evaluations, other methods, such as measuring the magnetic susceptibility, can be used. Second, this protocol allows for the detection of pile-up artifacts (as an indicator of slice distortions) only directly adjacent to the signal loss artifact. However, additional slice distortions can be expected beyond the signal loss artifact as well. That is why it is likely that the amount of distortions is underestimated.

In conclusion, this protocol can help to standardize future studies evaluating the MRI artifact volume of implants and the vulnerability of pulse sequences to metallic artifacts. This might help to optimize the MRI suitability of implants and sequence techniques to finally improve patient care.

Disclosures

Tim Hilgenfeld, Franz S. Schwindling, and Alexander Juerchott received funding from a postdoctoral fellowship of the Medical Faculty of the University of Heidelberg. The study was supported in part by the Dietmar-Hopp-Stiftung (project no. 23011228). The authors have stated explicitly that there are no conflicts of interest in connection with this article.

Acknowledgements

The authors like to thank Stefanie Sauer, pharmacist at the Department of Pharmacy Heidelberg University Hospital, for her contributions to the MRI phantom. In addition, we would like to thank NORAS MRI products GmbH (Höchberg, Germany) and especially Daniel Gareis for providing a prototype of the 16-channel multipurpose coil. Furthermore, we are grateful for the kind cooperation with SIEMENS Healthcare GmbH (Erlangen, Germany) and especially Mathias Nittka for their assistance in the sequence setup.

References

1. Matsumoto, M., Koike, S., Kashima, S., Awai, K. Geographic distribution of CT, MRI and PET devices in Japan: a longitudinal analysis based on national census data. *PLoS ONE*. **10** (5) (2015).
2. Cram, P. *et al.* Total knee arthroplasty volume, utilization, and outcomes among medicare beneficiaries, 1991-2010. *JAMA*. **308** (12), 1227-1236 (2012).
3. Jordan, R. A., Micheelis, W. *Fünfte Deutsche Mundgesundheitsstudie (DMS V).* Deutscher Zahnärzte Verlag DÄV. Köln (2016).
4. Steiner, C., Andrews, R., Barrett, M., Weiss, A. *HCUP projections mobility/orthopedic procedures 2003 to 2012*: *Report #2012-03.* U.S. Agency for Healthcare Research and Quality. Rockville (2012).
5. Kremers, H. *et al.* Prevalence of total hip and knee replacement in the United States. *The Journal of Bone and Joint Surgery.* **97** (17), 1386-1397 (2015).
6. Schenck, J. The role of magnetic susceptibility in magnetic resonance imaging: MRI magnetic compatibility of the first and second kinds. *Medical Physics.* **23** (6), 815-850 (1996).
7. Filli, L. *et al.* Material-dependent implant artifact reduction using SEMAC-VAT and MAVRIC: a prospective MRI phantom study. *Investigative Radiology.* **52** (6), 381 (2017).
8. Klinke, T. *et al.* Artifacts in magnetic resonance imaging and computed tomography caused by dental materials. *PloS ONE.* **7** (2) (2012).
9. Lee, J. *et al.* Usefulness of IDEAL T2-weighted FSE and SPGR imaging in reducing metallic artifacts in the postoperative ankles with metallic hardware. *Skeletal Radiology.* **42** (2), 239-247 (2013).
10. Zho, S.-Y., Kim, M.-O., Lee, K.-W., Kim, D.-H. Artifact reduction from metallic dental materials in T1-weighted spin-echo imaging at 3.0 tesla. *Journal of Magnetic Resonance Imaging.* **37** (2), 471-478 (2013).
11. Fritz, J. *et al.* Compressed sensing SEMAC: 8-fold accelerated high resolution metal artifact reduction MRI of Cobalt-Chromium knee arthroplasty implants. *Investigative Radiology.* **51** (10), 666 (2016).
12. Aguiar, M., Marques, A., Carvalho, A., Cavalcanti, M. Accuracy of magnetic resonance imaging compared with computed tomography for implant planning. *Clinical Oral Implants Research.* **19** (4), 362-365 (2008).
13. Talbot, B. S., Weinberg, E. P. MR imaging with metal-suppression sequences for evaluation of total joint arthroplasty. *RadioGraphics.* **36** (1), 209-225 (2015).
14. Ai, T. *et al.* SEMAC-VAT and MSVAT-SPACE sequence strategies for metal artifact reduction in 1.5T magnetic resonance imaging. *Investigative Radiology.* **47** (5), 267-276 (2012).
15. Smeets, R. *et al.* Artefacts in multimodal imaging of titanium, zirconium and binary titanium-zirconium alloy dental implants: an *in vitro* study. *Dento Maxillo Facial Radiology.* **46** (2), 20160267 (2016).
16. Nawabi, D. H. *et al.* MRI predicts ALVAL and tissue damage in metal-on-metal hip arthroplasty. *Clinical Orthopaedics and Related Research.* **472** (2), 471-481 (2014).
17. Cooper, H. J. *et al.* Early reactive synovitis and osteolysis after total hip arthroplasty. *Clinical Orthopaedics and Related Research.* **468** (12), 3278-3285 (2010).

